A Power-Domain MST Scheme With BPPM in NLOS Ultraviolet Communications

Tian Cao ⬤, *Graduate Student Member, IEEE*, Tianfeng Wu, *Graduate Student Member, IEEE*,
Changyong Pan, *Senior Member, IEEE*, and Jian Song ⬤, *Fellow, IEEE*

Abstract—Due to the high path loss of non-line-of-sight (NLOS) ultraviolet communications (UVC) channel, pulse modulation schemes, such as on-off keying (OOK) and M-ary pulse-position modulation (PPM), and photon-counting receivers are commonly adopted. Although M-ary PPM can be demodulated and decoded without the channel state information, its spectral efficiency is lower than OOK's. To improve the spectral efficiency of M-ary PPM in NLOS UVC, a power-domain multilayer-superposed transmission (MST) scheme with binary PPM (BPPM) is proposed in this work. Based on this scheme, the signal in each layer can be directly decoded without successive interference cancellation, which is necessary for other MST schemes in the power domain. Hence, a low complexity receiver in the NLOS UVC system can be realized. Additionally, the bit-error rate (BER) and achievable data rate (ADR) expressions of the proposed MST scheme are derived. Monte-Carlo simulations are performed to verify the analytical BER expression. The NLOS UVC system performance employing the proposed MST scheme is further demonstrated and compared with pure BPPM. The results indicate that with the optimal power allocation factor for each layer, the overall ADR of the NLOS UVC system with the proposed power-domain MST scheme can surpass that with pure BPPM.

Index Terms—Ultraviolet communications, non-line-of-sight, multilayer-superposed transmission scheme, binary pulse-position modulation.

I. INTRODUCTION

DUE to the shorter wavelength of the ultraviolet (UV) light than that of infrared and visible light, the strong scattering effect of the UV light caused by atmospheric molecules and aerosols enables non-line-of-sight (NLOS) ultraviolet communications (UVC) [1], [2]. Admittedly, an NLOS UVC link would face high path loss, resulting in less optical power being collected by the receiver. However, the solar radiation in the spectral region of the so-called solar-blind UV light from 200 to 280 nm is blocked by ozone in the upper atmosphere [3], [4]. Extremely low background noise can be achieved by detectors on the ground. Under this condition, high-gain photomultiplier tubes (PMT) are commonly adopted to detect optical signals, by which quantum noise-limited photon-counting detection can be approached [5]. That is, an arrived photon would be converted to a photoelectron pulse by the PMT given the quantum efficiency. The optical signal is converted to a series of photoelectron pulses. By counting the number of photoelectron pulses in each slot of the signal, the transmitted information can be recovered and that is why it is called photon-counting receiver (PCR). Therefore, pulse modulations, such as on-off keying (OOK) and M-ary pulse-position modulation (PPM), are commonly adopted in practical NLOS UVC systems in recent decades [5], [6], [7], [8], [9], [10], [11]. OOK is a binary pulse-amplitude modulation that is easy to analyze. However, channel state information (CSI) is required in demodulating the OOK signal in order to find a suitable threshold to minimize the bit-error rate (BER) [12]. Compared with OOK, M-ary PPM does not have the aforementioned drawback. This is because the M-ary PPM signal can be demodulated via the soft-decision decoding (SDD) scheme, where the decoder will select the slot with the maximum number of photoelectron pulses as the pulsed slot in an M-ary PPM symbol [13]. However, the spectral efficiency of M-ary PPM is lower than that of OOK especially as the number of slots in an M-ary PPM symbol increases. In order to relieve this problem, multipulse pulse-position modulation (MPPM) has been proposed and widely studied [14], [15]. Nevertheless, the number of possible constellation points of MPPM is not a power of two, which will increase the complexity in bit-to-symbol mapping and demapping [16].

In this work, we aim to exploit the advantage of M-ary PPM while enhancing its spectral efficiency in NLOS UVC systems. Different from MPPM by increasing the number of pulses during a symbol to convey more information, we attempt to superpose the M-ary PPM symbols in the power domain to convey more information at the identical time, spectral, and spatial resources, which refers to the power-domain multilayer-superposed transmission (MST) scheme. To date, a few works regarding the power-domain MST scheme in NLOS UVC systems have been

Tian Cao and Tianfeng Wu are with the Beijing National Research Center for Information Science and Technology (BNRist), Department of Electronic Engineering, Tsinghua University, Beijing 100084, China (e-mail: caot19@mails.tsinghua.edu.cn; wtf22@mails.tsinghua.edu.cn).

Changyong Pan is with the Beijing National Research Center for Information Science and Technology (BNRist), Department of Electronic Engineering, Tsinghua University, Beijing 100084, China, and also with Key Laboratory of Digital TV System of Shenzhen City, Research Institute of Tsinghua University, Shenzhen 518057, China (e-mail: pcy@tsinghua.edu.cn).

Jian Song is with the Beijing National Research Center for Information Science and Technology (BNRist), Department of Electronic Engineering, Tsinghua University, Beijing 100084, China, and with the Key Laboratory of Digital TV System of Shenzhen City, Research Institute of Tsinghua University, Shenzhen 518057, China, and also with Shenzhen International Graduate School, Tsinghua University, Shenzhen 518055, China (e-mail: jsong@tsinghua.edu.cn).

reported. In [17], the error performance of the power-domain MST scheme with OOK in NLOS UVC systems was investigated. In that work, the authors assumed that perfect successive interference cancellation (SIC) is achieved in decoding the current layer by capacity-approaching codes; thus, all the re-encoded symbols for decoding the subsequent layers are correct. In addition, maximum-likelihood (ML) detection was adopted to detect the bits modulated by the OOK in each layer. The CSI, hence, is indispensable. In [18], the authors proposed channel estimation and symbol decoding algorithms for the power-domain MST scheme with OOK in NLOS UVC systems under the condition that the symbol boundaries on different signal layers may not be aligned in the time domain. The error performances of their proposed algorithms were demonstrated by numerical simulations and experiments. However, the aforementioned works only use OOK, whereas M-ary PPM has not been studied in the power-domain MST scheme, to the best of our knowledge. In addition, they exclusively focus on the error performance of the power-domain MST scheme with OOK in NLOS UVC systems.

Motivated by the aforementioned investigation, we put forward a power-domain MST scheme with binary pulse-position modulation (BPPM) to enhance the spectral efficiency of M-ary PPM in NLOS UVC systems. It is shown in [12] that the spectral efficiency of ternary PPM is the highest but the number of constellation points is 3, not a power of two. Therefore, BPPM is taken into account since its spectral efficiency is the second highest among other M-ary PPM. Specifically, the coding and decoding processes of the proposed MST scheme are illustrated in detail. The designed coding method can realize variable bit-rate transmissions in different layers. The designed decoding method can directly recover the information of the BPPM signal in each layer without SIC. In addition, the threshold is not required anymore in the designed decoding method; thus, the CSI is not necessary. Furthermore, the analytical BER and achievable data rate (ADR) expressions are derived. Monte-Carlo (MC) simulations are provided to verify the analytical results. By formulating the optimization problem to get the maximum overall ADR, the power allocation factor (PAF) of each layer is obtained. Finally, the overall ADR performances of the proposed MST scheme are compared with the BPPM.

II. NLOS UVC CHANNEL AND POWER-DOMAIN MST SYSTEM MODEL

The considered UVC system with a transmitter (Tx) and a receiver (Rx) is illustrated in Fig. 1. The Tx and Rx locate at the origin and the coordinates $(0, r, 0)$, hence the vector from the Tx to the Rx is $\mathbf{r} = [0, r, 0]^{\mathrm{T}}$, where the superscript "T" represents the transpose operator. The Tx equips a UV light-emitting diode (LED), which is driven by an LED driver with the input of an N-layer superposed electrical signal. The emission pattern of the UV LED follows Lambertian distribution, which is given as follows

$$\mathcal{L}(\mu) = \begin{cases} \frac{m_L+1}{2\pi} \mu^{m_L}, & 0 \leq \gamma_T \leq \frac{\pi}{2} \\ 0, & \frac{\pi}{2} < \gamma_T \leq \pi \end{cases}, \qquad (1)$$

where $\mu = \cos \gamma_T$, γ_T is the angle between $\boldsymbol{\mu}_T$ and $\mathbf{r}_1$. $\boldsymbol{\mu}_T = [\sin \theta_T \cos \phi_T, \sin \theta_T \sin \phi_T, \cos \theta_T]^{\mathrm{T}}$ is the direction vector of
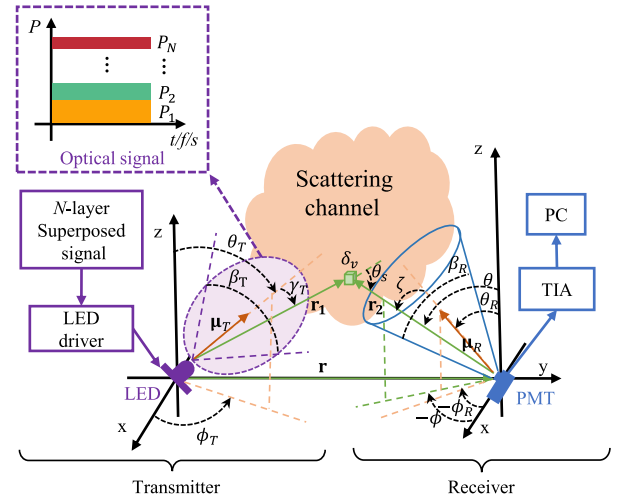

Fig. 1. The diagram of an NLOS UVC system using the proposed MST scheme with N layers in the power domain.

the LED, where θ_T and ϕ_T are the inclination and the azimuth angles of the LED at the Tx, respectively. $\mathbf{r}_1$ is the vector from the LED to the δ_v, which is the infinitesimal volume wrapping an arbitrary scattering point in the PMT's field-of-view (FOV). The shape of the PMT's FOV is assumed to be conical and the corresponding full FOV angle is denoted by β_R. m_L is the order of Lambertian emission and can be obtained as $-\frac{\ln 2}{\ln \cos(\beta_T/2)}$, where β_T denotes the full angle at the half illuminance of the UV LED. The emitted optical signal consists of N layers. The average optical power of layer n (L_n) is P_n, $n = 1, 2, \ldots, N$. Those N layers are superposed in the power domain and transmitted utilizing identical time, spectral, and spatial resources. Through the atmospheric scattering channel, Rx can receive the optical signal emitted by the Tx via NLOS links. Due to the significant scattering loss but extremely low background noise in the solar-blind UV window [3], Rx adopts an ideal PCR, which can be practically realized by connecting a PMT to a trans-impedance amplifier (TIA), whose output signal is then passed to a photon counter (PC) [19]. The inclination and the azimuth angles of the PMT at the Rx is set to θ_R and ϕ_R, respectively, and the corresponding direction vector is $\boldsymbol{\mu}_R = [\sin \theta_R \cos \phi_R, \sin \theta_R \sin \phi_R, \cos \theta_R]^{\mathrm{T}}$.

A. Channel Model

Due to the huge path loss by the multiple-order scattering in the NLOS UVC channel, the received optical power from the first-order scattering could be a hundred times higher than that from the multiple-order scattering, especially in the short-range communications scenarios that NLOS UVC systems are mainly designed to [3], [20], [21], [22]. Therefore, the channel gain of the NLOS UVC systems is dominated by the received optical power via the first-order scattering. Since NLOS UVC is always exploited as a short-range communication solution with LEDs adopted as light sources in practical applications, the effect of turbulence on the UV light is ignored [23], [24], [25]. In this work, a very recently proposed single-scatter path loss model using an LED as the light source [26] is adopted to assess the channel gain between the Tx and the Rx. In accordance with [26],

the channel gain can be written as

$$h = \int_{\theta_{\min}}^{\theta_{\max}} \int_{\phi_{\min}}^{\phi_{\max}} \int_{r_{2\min}}^{r_{2\max}} k_s A_r \exp\left[-k_e \left(r_1 + r_2\right)\right]$$

$$\times \frac{\cos\zeta \mathcal{L}\left(\mu\right) \mathcal{P}\left(\upsilon\right)}{r_1^2} \sin\theta \mathrm{d}\theta \mathrm{d}\phi \mathrm{d}r_2, \tag{2}$$

where k_s is the scattering coefficient. $k_e = k_s + k_a$ is the extinction coefficient and k_a is the absorption coefficient. A_r is the detection area of the PMT. $r_1 = \|\mathbf{r}_1\|$ and $r_2 = \|\mathbf{r}_2\|$, where $\mathbf{r}_2$ is the vector from the PMT to the δ_v. $\mathcal{P}(\upsilon)$ is the scattering phase function and can be expressed as the weighted sum of Rayleigh and Mie scattering functions ($\mathcal{P}_{Ray}(\upsilon)$ and $\mathcal{P}_{Mie}(\upsilon)$), that is,

$$\mathcal{P}\left(\upsilon\right) = \frac{k_{Mie}}{k_s} \mathcal{P}_{Mie}\left(\upsilon\right) + \frac{k_{Ray}}{k_s} \mathcal{P}_{Ray}\left(\upsilon\right), \tag{3}$$

where υ equals $\cos\theta_s$, and θ_s is the scattering angle. $k_s = k_{Mie} + k_{Ray}$; k_{Mie} and k_{Ray} are the Mie and the Rayleigh scattering coefficients, respectively. $\mathcal{P}_{Ray}(\upsilon)$ and $\mathcal{P}_{Mie}(\upsilon)$ can be expressed as [27], [28]

$$\mathcal{P}_{Ray}\left(\upsilon\right) = \frac{3\left[1 + 3\gamma + \left(1 - \gamma\right)\upsilon^2\right]}{16\pi\left(1 + 2\gamma\right)} \tag{4}$$

and

$$\mathcal{P}_{Mie}\left(\upsilon\right) = \frac{1 - g^2}{4\pi}\left[\frac{1}{\left(1 + g^2 - 2g\upsilon\right)^{\frac{3}{2}}} + \frac{f\left(3\upsilon^2 - 1\right)}{2(1 + g^2)^{\frac{3}{2}}}\right], \tag{5}$$

respectively, where γ, g, and f are atmospheric model parameters. The way of calculating the integral limits of θ, ϕ, and r_2 of (2) can be found in [26].

Furthermore, the channel impulse response (CIR) of the single-scatter NLOS UVC channel can be written as [29]

$$h_s(t) = Q_T k_s \int_{\theta_{\min}}^{\theta_{\max}} \int_{\phi_{\min}}^{\phi_{\max}} \varphi\left(t, \theta, \phi\right) \mathrm{d}\theta \mathrm{d}\phi, \tag{6}$$

where

$$\varphi\left(t, \theta, \phi\right) = \begin{cases} \frac{\mathcal{L}(\mu)\exp[-k_e(r_1+\tilde{r}_2(t))]\cos\zeta\mathcal{P}(\upsilon)\sin\theta}{r_1^2}\tilde{r}_2'(t), \\ \qquad \tilde{t}\left(r_{2\min}\right) < t \leq \tilde{t}\left(r_{2\max}\right) \\ 0, \qquad\qquad\qquad \text{otherwise} \end{cases} \tag{7}$$

$\tilde{t}(r_2) = \frac{r_1+r_2}{c}$, $\tilde{r}_2'(t)$ is the first-order derivative of $\tilde{r}_2(t) = \frac{(ct)^2 - r^2}{2ct + 2r\sin\theta\sin\phi}$, and Q_T is the energy of an optical impulse transmitted at time 0. Without loss of generality, we set Q_T to 1 J. Finally, applying Fourier transform to $h_s(t)$, the channel frequency response $H_s(f)$ can be obtained as

$$H_s(f) = \int_{-\infty}^{+\infty} h_s(t) \exp\left(-j2\pi ft\right) \mathrm{d}t, \tag{8}$$

where j is the imaginary unit.

B. Implementation of the Proposed Power-Domain MST Scheme

In this subsection, the power-domain MST scheme with BPPM adopted in each layer is illustrated. Considering the fact that a symbol of BPPM contains a pulsed slot and an unpulsed

slot, we propose to superpose an upper layer with two BPPM symbols onto the lower layer with one BPPM symbol. One of two BPPM symbols in the upper layer is superposed onto the pulsed slot of the BPPM symbol in the lower layer and the other in the unpulsed slot. Based on this idea, the number of layers in the proposed MST scheme can be extended. It is assumed that there are N layers superposed in the output optical signal of the LED, and the L_n utilizes the BPPM with the bit rate of $R_n, n = 1, 2, \ldots, N$. It can be obtained that $R_n = 2^{n-1}R_1$. Let $T_n = \frac{1}{R_n}$ be the symbol interval of a BPPM in the L_n. Hence, T_1 is the longest symbol interval among N layers. Let P_t be the total average optical transmission power of the LED and $\rho_n \in [0, 1]$ be the power allocation factor (PAF) of the L_n, we have $P_n = \rho_n P_t$ and $\sum_{n=1}^{N} \rho_n = 1$. Therefore, the signal of the L_n can be expressed as

$$x_n(t) = \sum_k \left[\left(1 - x_n[k]\right) g_p\left(t - kT_n; n\right)\right.$$

$$\left. + x_n[k]g_p\left(t - \frac{T_n}{2} - kT_n; n\right)\right], \tag{9}$$

where $x_n[k]$ is the k-th bit in the x_n, which is the bitstream in the L_n. $g_p(t; n)$ is the pulse shaping function for the L_n and defined as

$$g_p\left(t; n\right) = \begin{cases} 2P_n/\mathcal{G}, & 0 \leq t \leq \frac{T_n}{2} \\ 0, & \text{otherwise} \end{cases}, \tag{10}$$

where $\mathcal{G}$ denotes the current-to-light conversion efficiency of LED with the unit of W/A [30]. By superposing all signals of N layers, the output optical signal of the LED can be expressed as

$$x(t) = \mathcal{G} \sum_{n=1}^{N} x_n(t). \tag{11}$$

Since the LEDs in optical communication systems are supposed to work in the linear region where $\mathcal{G}$ nearly remains a constant [30]. Therefore, we set $\mathcal{G}$ to one hereinafter for clear presentation.

Furthermore, the electrical power spectrum of the proposed MST scheme is analyzed. According to the power spectrum of BPPM given in [31], the power spectrum of the signal in the L_n can be expressed as

$$S_n(f) = |G_p\left(f; n\right)|^2 \left[\frac{2\pi}{T_n}\left(\frac{1}{2} - \frac{1}{2}\cos\left(\pi fT_n\right)\right)\right.$$

$$\left. + \left(\frac{2\pi}{T_n}\right)^2 \sum_{k=-\infty}^{+\infty} \delta\left(f - \frac{2k}{T_n}\right)\right], \tag{12}$$

where $\delta(\cdot)$ is the Dirac delta function, $G_p(f; n)$ is the Fourier transform of the pulse shape. Based on the pulse shaping function defined in (10), $G_p(f; n)$ can be obtained as

$$G_p\left(f; n\right) = P_n T_n \operatorname{sinc}\left(f\frac{T_n}{2}\right) \exp\left(-j\pi f\frac{T_n}{2}\right), \tag{13}$$

Furthermore, based on the Wiener–Khinchin theorem, the power spectrum of the proposed MST scheme can be further expressed
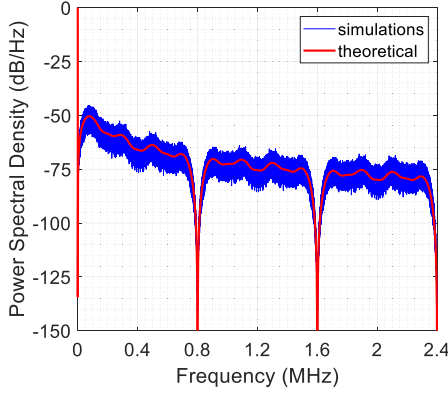
Fig. 2. Power spectral density of the proposed MST scheme with $N = 3$, $P_t = 1$, $\rho_1 = 0.5$, $\rho_2 = 0.3$, $\rho_3 = 0.2$, and $R_1 = 10^5$ bps.
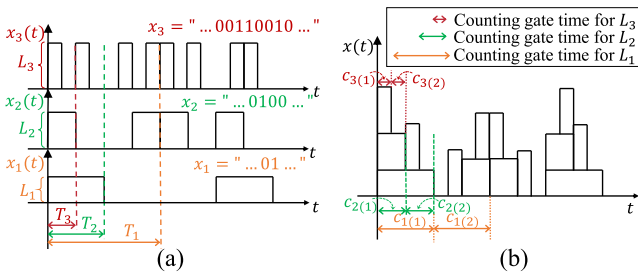

Fig. 3. Graphic representation of the proposed power-domain MST scheme with three layers. (a) Each layer in the output optical signal of the LED. (b) Decoding the signal of each layer at the Rx.

as

$$
S(f) = \sum_{n=1}^{N} S_n(f) + \delta(f) \sum_{i=1}^{N} \sum_{\substack{k=1 \\ k \neq i}}^{N} P_i P_k
$$

$$
= \sum_{n=1}^{N} \left[P_n T_n \operatorname{sinc}\left(f \frac{T_n}{2} \right) \right]^2 \left[\frac{\pi - \pi \cos(\pi f T_n)}{T_n} \right.
$$

$$
\left. + \left(\frac{2\pi}{T_n} \right)^2 \sum_{k=-\infty}^{+\infty} \delta\left(f - \frac{2k}{T_n} \right) \right] + \delta(f) \sum_{i=1}^{N} \sum_{\substack{k=1 \\ k \neq i}}^{N} P_i P_k.
$$

$$(14)$$

Fig. 2 gives both theoretical results and simulations of the power spectrum of the proposed MST scheme. Here, we set $P_t = 1$, $N = 3$, $R_1 = 10^5$ bps, $\rho_1 = 0.5$, $\rho_2 = 0.3$, and $\rho_3 = 0.2$. It can be seen from Fig. 2 that theoretical results match well with simulations, which verifies the theoretical expression in (14). Additionally, it can be found from Fig. 2 that the first null locates at 0.8 MHz, which is the double of the bit rate of L_3. This manifests that the bandwidth from direct current (DC) to the first null of the proposed MST scheme is determined by the bit rate of the highest layer, i.e., R_N.

In Fig. 3(a), an example of MST scheme with three layers is presented. The bitstream of the L_1 is assumed to $x_1 = $ "$\ldots 01 \ldots$" in this example. Thus, for the first bit in the x_1, there

is a pulsed optical signal at the first slot of the BPPM symbol; And for the second bit in the x_1, there is a pulsed optical signal at the second slot of the BPPM symbol. It can be found that during the time of T_1, there are 1, 2, and 4 bits are transmitted in the L_1, L_2, and L_3, respectively. For example, when the first bit in the x_1 is transmitted, the first two bits in the x_2, i.e., "01," are transmitted simultaneously. Since the first bit in the x_1 is "0," the signal of the first bit in the x_2 locates at the pulsed slot of the first bit in the x_1, and the signal of the second bit in the x_2 locates at the unpulsed slot of the first bit in the x_1. In the same way, when the first bit in the x_2 is transmitted, the first two bits in the x_3, i.e., "00," are transmitted. The symbol duration offset is ignored in this work because the signals of different layers are superposed at the transmitter, where the transmission of symbols in each layer can be driven by the same hardware clock to easily avoid offset.

When the optical signal arrives at the Rx, it will be processed by a PCR. Commonly, in order to recover the information that L_n carried, Rx needs to reconstruct and then cancel the signals of L_n's former layers before decoding the signal of the L_n. This process is known as SIC, which would increase the complexity of the receiver and result in error propagation degrading the system performance [32]. In the proposed MST scheme, Rx can directly obtain the information carried by L_n. More specifically, assuming perfect synchronization is performed, the detected photons in the first and second slots of a BPPM symbol in the L_n are $c_{n(1)}$ and $c_{n(2)}$, respectively, obtained by setting the counting gate time of the PC to the half of the symbol interval in the L_n, i.e., $\frac{T_n}{2}$. If $c_{n(1)} > c_{n(2)}$, the received BPPM symbol is decoded as a "0" bit. If $c_{n(1)} < c_{n(2)}$, the received BPPM symbol is decoded as a "1" bit. When a tie occurs, i.e., $c_{n(1)} = c_{n(2)}$, the random choice of "0" or "1" bits will be made. The ground why the aforementioned decoding method for the proposed MST scheme can work relies on the fact that the signals of other layers, including upper and lower layers of the L_n, contribute the same optical energy to both two slots of a BPPM symbol in the L_n. In order to better illustrate this idea, Fig. 3(b) gives an example, where the superposed optical signal of three layers in Fig. 3(a) is provided. If Rx wants to decode the first bit in the L_2, by setting the counting gate time of the PC to $\frac{T_2}{2}$, it can get the photons in the first and second slots of the first BPPM symbol $c_{2(1)}$ and $c_{2(2)}$, respectively. It can be found that L_1 and L_3 contribute the optical energy of $\frac{P_1 T_1}{2}$ and $P_3 T_3$ to each slot of the first BPPM symbol in the L_2, respectively. Therefore, the difference in the number of detected photons between two slots of the first BPPM symbol in the L_2 depends on the bit sent by itself. That is why, in the proposed MST scheme, by comparing the number of detected photons in two slots can decode the BPPM symbol in the L_n.

C. System Model

The number of the detected photons (ε) during each slot of the BPPM symbol in the L_n is a random variable and can be expressed as $\varepsilon = x + z$, where x and z are the numbers of the detected signal photons and background noise photons in a slot, respectively. Both x and z obey the Poisson distribution, whose

probability mass function (PMF) is defined as follows

$$f_P(\xi; \lambda) = \frac{\lambda^\xi}{\xi!} \exp(-\lambda), \tag{15}$$

where ξ is the variable of the Poisson distribution and denotes the number of detected photons in a slot, λ is the average number of the detected photons per slot. The corresponding cumulative distribution function (CDF) can be obtained as

$$F_P(\xi; \lambda) = \sum_{i=0}^{\xi} \frac{\lambda^i}{i!} \exp(-\lambda). \tag{16}$$

The average number of detected signal photons in a slot of the BPPM symbol in the L_n can be expressed as

$$\mathcal{T}_n = \frac{h\eta}{Q_p} \int_{\frac{T_n}{2}} x(t)\mathrm{d}t, \tag{17}$$

where η is the total quantum efficiency of the PCR, $Q_p = h_p\nu$ is the energy of a photon, h_p is the Planck's constant, $\nu = c/\lambda_w$ is the frequency of the UV light, c is the speed of light, and λ_w is the wavelength of the UV light. Additionally, the average number of detected background noise photons in a slot of the BPPM symbol in the L_n can be expressed as

$$\lambda_n^b = \frac{\Lambda_b}{2R_n}, \tag{18}$$

where Λ_b is the background radiation photon rate.

III. Performance Analysis

In this section, the BER and ADR expressions of the NLOS UVC system using the proposed MST scheme with BPPM are derived. Here, we assume that "0" and "1" bits in the bitstream of each layer are equally distributed, that is, $\Pr(x_n[k] = 0) = \Pr(x_n[k] = 1) = \frac{1}{2}$. To clearly show the derivation of the BER and ADR expressions, the BPPM signal of the first bit in each layer will be taken into consideration, and the first bit in the L_n is denoted by $x_{(n)}$ for simple denotation hereinafter.

Since we need to compare the numbers of the detected photons in the first and second slots of a BPPM symbol during decoding it in the L_n, the average numbers of the detected photons in the first and second slots, which are denoted by $\lambda_{n|1}$ and $\lambda_{n|2}$, respectively, need to derive at first. Because the bits sent in each layer are random, $\lambda_{n|1}$ and $\lambda_{n|2}$ are both discrete random variables, the PMFs of which are given in the Lemma 1.

Lemma 1: The PMFs of $\lambda_{n|1}$ and $\lambda_{n|2}$ can be obtained as

$$f_{\lambda_{n|1}}\left(\lambda_{n|1} = \mathcal{T}_{n|1}(x_{(1)}, \ldots, x_{(n)}) + \lambda_n^b\right) = \frac{1}{2^n} \tag{19}$$

and

$$f_{\lambda_{n|2}}\left(\lambda_{n|2} = \mathcal{T}_{n|2}(x_{(1)}, \ldots, x_{(n)}) + \lambda_n^b\right) = \frac{1}{2^n}, \tag{20}$$

respectively, where

$$\mathcal{T}_{n|1}(x_{(1)}, \ldots, x_{(n)})$$
$$= \frac{h\eta}{R_n Q_p}\left(\sum_{i=n+1}^{N} \frac{P_i}{2} + \sum_{j=1}^{n}\left(1 - x_{(j)}\right)P_j\right) \tag{21}$$

is the average number of the detected signal photons in the first slot of a BPPM symbol in the L_n and

$$\mathcal{T}_{n|2}(x_{(1)}, \ldots, x_{(n)})$$
$$= \frac{h\eta}{R_n Q_p}\left(\sum_{i=n+1}^{N} \frac{P_i}{2} + x_{(n)}P_n + \sum_{j=1}^{n-1}\left(1 - x_{(j)}\right)P_j\right) \tag{22}$$

is the average number of the detected signal photons in the second slot of a BPPM symbol in the L_n

Proof: Please refer to Appendix A. ∎

It should be noted that both $\lambda_{n|1}$ and $\lambda_{n|2}$ are determined by $x_{(1)}, \ldots, x_{(n)}$. If $x_{(1)}, \ldots, x_{(n)}$ are specified, $\lambda_{n|1}$ and $\lambda_{n|2}$ are totally correlated. That is, we have the following corollary.

Corollary 1: The joint PMF of $\lambda_{n|1}$ and $\lambda_{n|2}$ can be written as

$$f_{\lambda_{n|1}, \lambda_{n|2}}\left(\lambda_{n|1} = \mathcal{T}_{n|1}(x_{(1)}, \ldots, x_{(n)}) + \lambda_n^b, \right.$$
$$\left.\lambda_{n|2} = \mathcal{T}_{n|2}(x_{(1)}, \ldots, x_{(n)}) + \lambda_n^b\right)$$
$$= f_{\lambda_{n|1}}\left(\lambda_{n|1} = \mathcal{T}_{n|1}(x_{(1)}, \ldots, x_{(n)}) + \lambda_n^b\right)$$
$$= f_{\lambda_{n|2}}\left(\lambda_{n|2} = \mathcal{T}_{n|2}(x_{(1)}, \ldots, x_{(n)}) + \lambda_n^b\right)$$
$$= \frac{1}{2^n} \tag{23}$$

Based on Lemma 1 and Corollary 1, the BER expression of the proposed MST scheme is given in the following Theorem.

Theorem 1: the BER expression of the L_n in the NLOS UVC system with the proposed MST scheme can be derived as (24) shown at the bottom of the next page, where $\mathcal{A}_1(x_{(1)}, \ldots, x_{(n-1)}) = \omega_S + \omega_I(x_{(1)}, \ldots, x_{(n-1)}) + \lambda_n^b$ and $\mathcal{A}_2(x_{(1)}, \ldots, x_{(n-1)}) = \omega_I(x_{(1)}, \ldots, x_{(n-1)}) + \lambda_n^b$. $\omega_S = \frac{h\eta P_n}{R_n Q_p}$ is the average number of the detected photons caused by the pulsed slot of a BPPM symbol in the L_n. $\omega_I(x_{(1)}, \ldots, x_{(n-1)}) = \frac{h\eta}{R_n Q_p}[\sum_{i=n+1}^{N} \frac{P_i}{2} + \sum_{j=1}^{n-1}(1 - x_{(j)})P_j]$ can be considered as the inference, which is the average number of the detected photons from other layers.

Proof: Please refer to Appendix B. ∎

By considering the channel as the binary discrete memoryless channel, the information that a BPPM symbol in the L_n can convey is able to be described by the mutual information as $1 - \mathcal{H}[P_e(n)]$ bits per symbol, where $\mathcal{H}(p) = -p\log_2(p) - (1-p)\log_2(1-p)$ is the binary entropy function [33]. Hence the ADR can be represented by the mutual information. For pulse modulations, the bandwidth is roughly proportional to the inverse of the slot width [34], which is also demonstrated in Fig. 2. That is, the shorter slot width is, the larger bandwidth is. Considering that the proposed MST is aimed to improve the bandwidth efficiency, for fairly demonstrating its improvements in the NLOS UVC systems, the ADR should be normalized to the minimum slot width of N layers, which is the slot width of the L_N. Therefore, based on Theorem 1, the overall ADR expression of the NLOS UVC system with the proposed MST scheme is provided in the following Theorem.

Theorem 2: Given that there are $\frac{2R_N}{R_n}$ minimum slots in a BPPM symbol, the overall ADR with the unit of bits per minimum slot (BPMS) of the NLOS UVC system with the proposed

TABLE I
THE CHANNEL GAINS OF THE NLOS UVC LINK AT DIFFERENT RANGES
BETWEEN THE TX AND THE RX

Range (m)	10	20	30	40	50
Channel gain ($\times 10^{-10}$)	4.812	2.369	1.555	1.148	0.904
Range (m)	60	70	80	90	100
Channel gain ($\times 10^{-10}$)	0.742	0.626	0.539	0.472	0.418

MST scheme can be obtained as

$$\mathcal{R}^o = \sum_{n=1}^{N} \mathcal{R}(n), \tag{25}$$

where $\mathcal{R}(n)$ is the ADR of the L_n of the proposed MST scheme and can be expressed as

$$\mathcal{R}(n) = \frac{R_n}{2R_N} \left(1 - \mathcal{H}\left[P_e(n)\right]\right)$$

$$= \frac{R_n}{2R_N} \{P_e(n)\log_2\left[2P_e(n)\right]$$

$$+ \left(1 - P_e(n)\right)\log_2\left[2\left(1 - P_e(n)\right)\right]\}. \tag{26}$$

In order to maximize the overall ADR, the PAF of each layer is obtained via the following optimization problem

$$\arg\max_{\rho_n} \quad \mathcal{R}^o$$

$$\text{s.t.} \quad \sum_{n=1}^{N} \rho_n = 1 \tag{27}$$

$$\rho_n \in [0, 1], \ n = 1, \ldots, N$$

This optimization problem can be efficiently solved by the standard solvers embedded in the MATLAB.

IV. RESULTS AND DISCUSSION

In this section, the performances of NLOS UVC systems with the proposed power-domain MST scheme are demonstrated. The parameters used in the calculation are extracted from the experimental setups and results in [11], [26], provided as follows: $\beta_T = 30°$, $\theta_T = 60°$, $\phi_T = 90°$, $\lambda_w = 266$ nm, $k_{Ray} = 0.24$ km^{-1}, $k_{Mie} = 0.25$ km^{-1}, $k_a = 0.9$ km^{-1}, $\gamma = 0.017$, $g = 0.72$, $f = 0.5$, $\Lambda_b = 14500$ sec^{-1}, $A_r = 1.92$ cm^2, $\eta = 0.1$, $\beta_R = 30°$, $\theta_R = 60°$, $\phi_R = -90°$. Since the short-range NLOS UVC is investigated in this work, the distances between the transceivers from 10 m to 100 m are considered in calculations. The channel gains calculated through (2) are shown in Table I. Additionally, the temporal and frequency characteristics of the considered NLOS UVC channel are demonstrated in Fig. 4. Fig. 4(a) and (b)
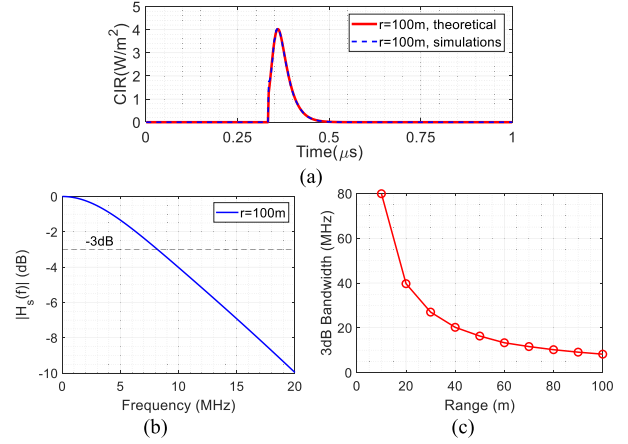

Fig. 4. The temporal and frequency characteristics of the NLOS UVC channel. (a) The CIR of the NLOS UVC channel with $r = 100$ m. (b) The frequency response of the NLOS UVC channel with $r = 100$ m. (c) 3 dB bandwidth versus the range between the Tx and the Rx.

exhibit the CIR and the corresponding frequency response of the NLOS UVC channel, respectively, when the range between the Tx and the Rx equals 100 m. The theoretical results in Fig. 4(a) are obtained via (6) and the corresponding simulations results are based on the methods in [22]. The amplitude of the frequency response at the DC in Fig. 4(b) is normalized to one making the determination of the 3 dB bandwidth easier. It can be found that the 3 dB bandwidth in Fig. 4(b) is about 8 MHz. Furthermore, the 3 dB bandwidth of the NLOS UVC channel against the range is given in Fig. 4(c). It can be found that with the increase of range, the 3 dB bandwidth decreases. Therefore, inter-symbol interference (ISI) can be safely ignored if the bit rate of the highest layer is less than 4 Mbps.

The performances of the NLOS UVC system with the proposed power-domain MST scheme versus the range between the Tx and Rx are given in Fig. 5 under the two- and three-layer conditions. P_t and R_1 are set to 0.2 W and 10^5 bps, respectively. For fair comparison, the BER and ADR results of BPPM with the minimum slot interval of the proposed MST scheme and the average optical power equaling P_t are provided. It can be seen in Fig. 5(a) and (d) that with the increase of the range, the optical power allocated to lower layer becomes less and that to higher layer becomes more. This is because with the increase of the range, the channel gain decreases and less optical power will be collected by the Rx. Under this condition, allocating more optical power to the higher layer could achieve better overall ADR. Furthermore, the MC simulation results of BER are also provided in Fig. 5(b) and (e). It can be found that the analytical results of BER match well with the corresponding MC simulation

$$P_e(n) = \frac{1}{2^{n-1}} \sum_{x_{(1)}=0}^{1} \cdots \sum_{x_{(n-1)}=0}^{1} \sum_{\varepsilon=0}^{+\infty} \frac{\mathcal{A}_2\left(x_{(1)}, \ldots, x_{(n-1)}\right)^{\varepsilon}}{\varepsilon!} \exp\left[-\mathcal{A}_2\left(x_{(1)}, \ldots, x_{(n-1)}\right)\right]$$

$$\times \left\{ \frac{\mathcal{A}_1\left(x_{(1)}, \ldots, x_{(n-1)}\right)^{\varepsilon}}{2\left(\varepsilon!\right)} \exp\left[-\mathcal{A}_1\left(x_{(1)}, \ldots, x_{(n-1)}\right)\right] + \sum_{i=0}^{\varepsilon-1} \frac{\mathcal{A}_1\left(x_{(1)}, \ldots, x_{(n-1)}\right)^{i}}{i!} \exp\left[-\mathcal{A}_1\left(x_{(1)}, \ldots, x_{(n-1)}\right)\right] \right\} \tag{24}$$
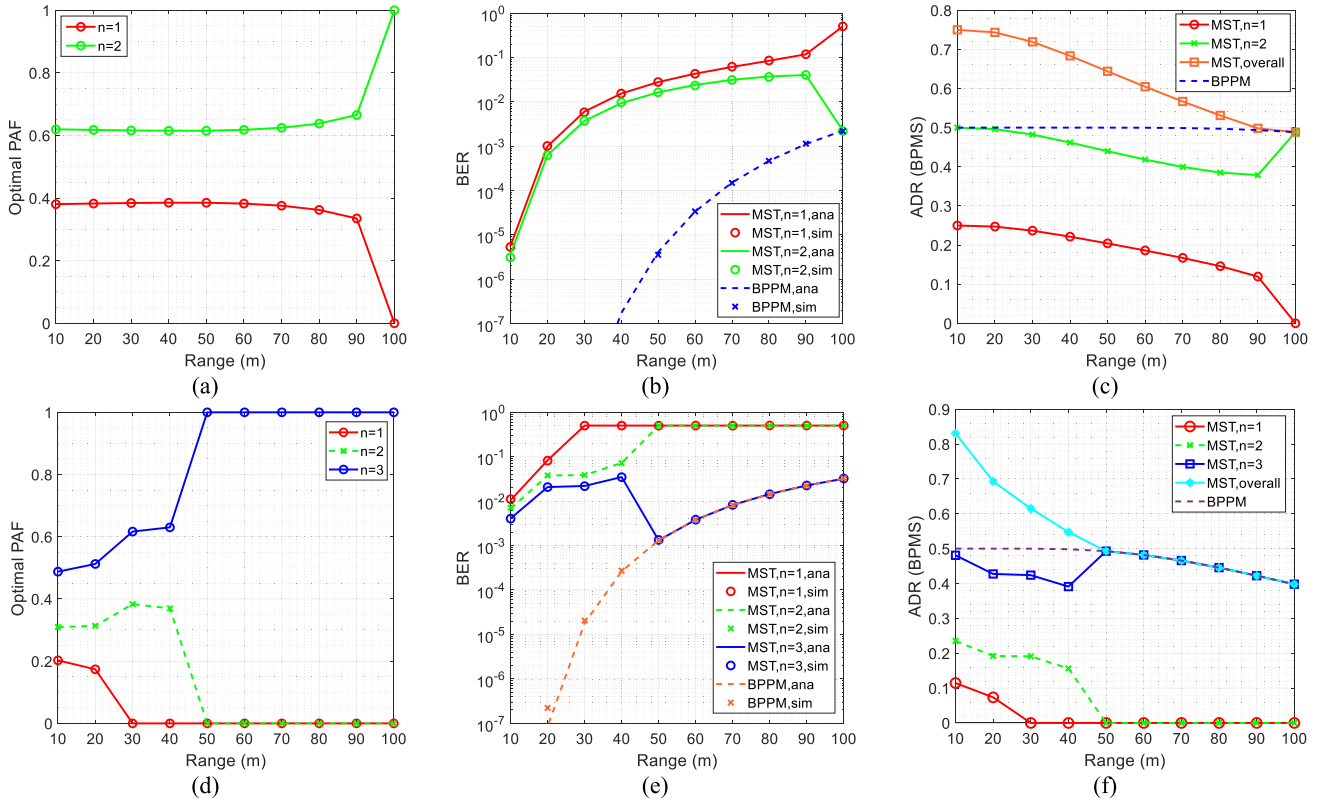
Fig. 5. Performances of the NLOS UVC system using the proposed power-domain MST scheme with two and three layers versus the range between the Tx and the Rx are compared with those of BPPM. (a), (b), and (c) give the optimal PAF, BER, and ADR of the two-layer case, respectively. (d), (e), and (f) provide the optimal PAF, BER, and ADR of the three-layer case, respectively. The optical transmission power (P_t) is set to 0.2 W. The data rate of the L_1, L_2, and L_3 are set to 10^5 bps, 2×10^5 bps, and 4×10^5 bps, respectively.

results in both two- and three-layer cases, which verifies the correctness of the analytical expression of BER. In addition, as the range increases, the BER of highest layer approaches to that of BPPM, and the BER of lower layers approaches to 0.5. This is because with the increase of range, the power allocated to the lower layers becomes less and approaches 0, whereas that to the highest layer becomes more and gets close to P_t. Therefore, as the range increases, the proposed power-domain MST scheme with the power allocation strategy in (26) would degenerate to the BPPM scheme with the minimum slot interval of the MST scheme. Moreover, in Fig. 5(c) and (f), the overall ADR of the proposed power-domain MST scheme increasingly approaches that of BPPM as the range increases for the same reason. However, when the range is short and hence the received optical power is improved, the overall ADR performance of the proposed power-domain MST scheme could be higher than that of BPPM. For example, when $r = 10$ m, the values of the overall ADR of the proposed power-domain MST scheme are about 0.75 and 0.84 BPMS in Fig. 5(c) and (f), respectively, whereas that of BPPM is 0.5 BPMS. This is because when the optical power allocated to the highest layer is enough, the spare optical power can be allocated to lower layers, leading to higher overall ADR. Therefore, the proposed power-domain MST scheme is more flexible and could achieve better spectral efficiency compared with BPPM.

The ADR performances of two- and three-layer cases with the same minimum slot interval, i.e., R_2 in the two-layer case equals R_3 in the three-layer case, and range are provided in the following Fig. 6. Here, R_2 in the two-layer case and R_3 in the three-layer case are set to 4×10^5 bps. The range between the Tx and the Rx is set to 50 m. The optimal PAFs for two- and three-layer cases are provided in Fig. 6(a) and (b), respectively. The corresponding overall ADR performances are further given in Fig. 6(c), where the ADR results of BPPM with the bit rate equaling 4×10^5 bps are also provided for comparison. We have already found in Fig. 5 that less collected optical power due to the increase of the range between the Tx and the Rx would result in more optical power being allocated to the highest layer. Here, we control the range and further reduce P_t. It can be seen from Fig. 6(a) and (b) that when P_t is smaller than about 0.2 W, the optical power will be allocated to one of N layers in the proposed power-domain MST scheme. Specifically, optical power is allocated from the highest layer to the lowest layer as P_t decreases. The proposed power-domain MST scheme with more layers could have more allocation choices to achieve better overall ADR performance under the condition that the minimum slot intervals are the same. This is because when P_t is low, the layer with large slot interval could collect more optical energy for one bit, hence the BER will reduce and the ADR will increase. Therefore, it can be found in Fig. 6(c) that the overall ADR
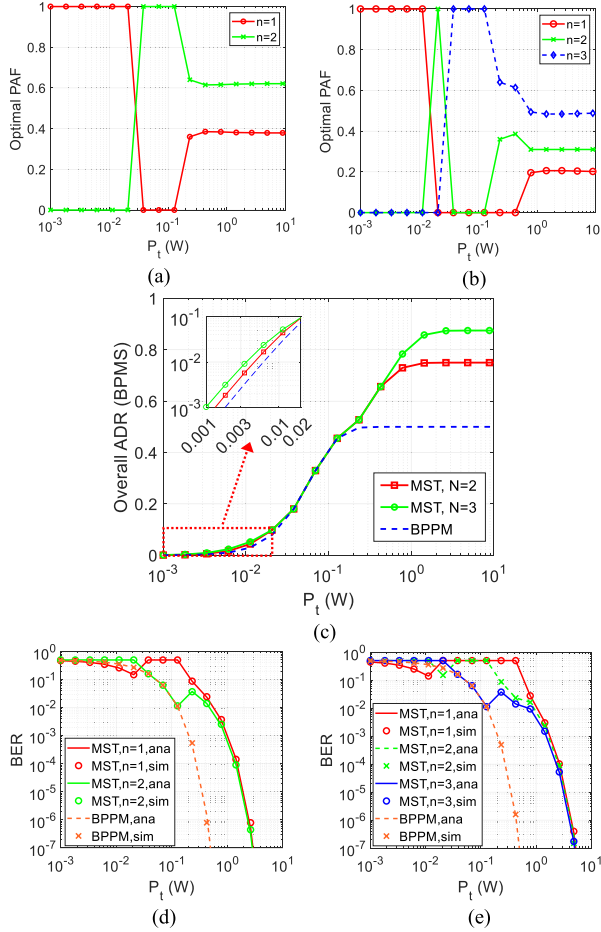
Fig. 6. With $r = 50$ m, (a) and (b) provide the optimal PAF of the proposed power-domain MST scheme in two- and three-layer cases, respectively. In the two-layer case, we set $R_1 = 2 \times 10^5$ bps and $R_2 = 4 \times 10^5$ bps. In the three-layer case, we set $R_1 = 10^5$ bps, $R_2 = 2 \times 10^5$ bps, and $R_3 = 4 \times 10^5$ bps. (c) further gives the overall ADR performance of the NLOS UVC system with the proposed power-domain MST scheme and BPPM. (d) and (e) demonstrate the BER performance of the proposed power-domain MST scheme in two- and three-layer cases, respectively.

performances of the proposed power-domain MST scheme with N of 2 and 3 are both better than or equal to that of BPPM, which can be regarded as a special case with $N = 1$ of the proposed power-domain MST scheme. The overall ADR results of the case with $N = 3$ are superior or equal to that with $N = 2$, because compared with the case of $N = 2$, the layer with lowest bit rate in the case of $N = 3$ can achieve better ADR performance and be selected to transmit information under the low-power condition, which manifests the flexibility of the proposed power-domain MST scheme. Furthermore, the results in Fig. 6(a) and (b) manifest that the optical power will be allocated to other layers when P_t exceeds about 0.2 W. At this time, BPPM almost achieves its own highest ADR, i.e., 0.5 BMPS, and will not increase anymore as the optical power increases. Whereas the overall ADR of the proposed power-domain MST scheme can be further enhanced, which indicates the superiority of the proposed power-domain MST scheme. Additionally, the BER of each layer in two- and three-layer cases are exhibited in Fig. 6(d) and (e), respectively. The BER results of BPPM are also given here for comparison. It

can be found from Fig. 6(c), (d), and (e) that although the overall ADR results of the proposed MST scheme outperform those of BPPM, the BER performance of each layer in the proposed MST scheme is worse than that of BPPM, especially when P_t is greater than 0.2 W. This is because the transmission power of each layer in the proposed MST scheme is less than that of BPPM. However, it can be observed from Fig. 6(d) and (e) that the slopes of the proposed MST scheme's BER curves are nearly the same as that of BPPM's as P_t increases. That is, the ability to mitigate the distortion of the proposed MST scheme is almost the same as that of BPPM.

V. CONCLUSION

In this paper, in order to enhance the spectral efficiency of M-ary PPM in NLOS UVC systems, a power-domain MST scheme with different bit-rate BPPM was proposed. The implementation of the proposed power-domain MST scheme was illustrated in detail, by which the signal in each layer can be decoded directly. Furthermore, the BER and ADR performances of the NLOS UVC system with proposed power-domain MST scheme were analytically investigated, and the corresponding expressions have been derived. The MC simulation results were provided to verify the correctness of the corresponding analytical results. The performances of NLOS UVC system with the proposed power-domain MST scheme were demonstrated and discussed. The results indicate that with the optimal PAFs, the proposed power-domain MST scheme is more flexible and can achieve higher spectral efficiency than pure BPPM. This work would be of help for designing and implementing the spectrally efficient NLOS UVC systems.

Although the ISI is neglected in this work because the considered bit rate is lower than the 3 dB bandwidth of the NLOS UVC channel, the bit rate can be further increased with high-power light sources adopted. Therefore, the effect of ISI will be studied in future work with high transmission power under the eye and skin exposure limits [3].

APPENDIX A
PROOF OF LEMMA 1

Based on the concept of the proposed MST scheme, it can be found that $\lambda_{n|1}$ and $\lambda_{n|2}$ consists of the average number of the background photons in the slot, i.e., λ_n^b and following three parts:

1) Let $\lambda_{n|1}^{(1)}$ and $\lambda_{n|2}^{(1)}$ be the average detected photons resulting from the optical signals transmitted in the upper layers in the first and second slots of a BPPM symbol in the L_n, respectively. Since the higher layers contribute the same optical energy to both two slots of a BPPM symbol in the L_n, $\lambda_{n|1}^{(1)}$ and $\lambda_{n|2}^{(1)}$ can be expressed as

$$\lambda_{n|1}^{(1)} = \lambda_{n|2}^{(1)} = \sum_{i=n+1}^{N} \frac{P_i h \eta}{2 R_n Q_p}. \tag{28}$$

2) Let $\lambda_{n|1}^{(2)}$ and $\lambda_{n|2}^{(2)}$ be the average detected photons resulting from the optical signal transmitted in its own layer in the

first and second slots of a BPPM symbol, respectively. Under this condition, they are determined by the sent bit. Therefore, it can be obtained that

$$\lambda_{n|1}^{(2)} = \left(1 - x_{(n)}\right) \frac{P_n h \eta}{R_n Q_p} \qquad (29)$$

and

$$\lambda_{n|2}^{(2)} = \frac{x_{(n)} P_n h \eta}{R_n Q_p}. \qquad (30)$$

3) Let $\lambda_{n|1}^{(3)}$ and $\lambda_{n|2}^{(3)}$ be the average detected photons resulting from the optical signals transmitted in the lower layers in the first and second slots of a BPPM symbol in the L_n, respectively. Since the lower layers also contribute the same optical energy to both two slots of a BPPM symbol in the L_n, $\lambda_{n|1}^{(3)}$ and $\lambda_{n|2}^{(3)}$ can be got as

$$\lambda_{n|1}^{(3)} = \lambda_{n|2}^{(3)} = \sum_{i=1}^{n-1} \left(1 - x_{(i)}\right) \frac{P_i h \eta}{R_n Q_p}. \qquad (31)$$

Therefore, the PMFs of $\lambda_{n|1}$ and $\lambda_{n|2}$ can be written as

$$f_{\lambda_{n|1}} \left(\lambda_{n|1} = \lambda_{n|1}^{(1)} + \lambda_{n|1}^{(2)} + \lambda_{n|1}^{(3)} + \lambda_n^b\right) = \prod_{i=1}^{n} \Pr\left(x_{(i)}\right) \qquad (32)$$

and

$$f_{\lambda_{n|2}} \left(\lambda_{n|2} = \lambda_{n|2}^{(1)} + \lambda_{n|2}^{(2)} + \lambda_{n|2}^{(3)} + \lambda_n^b\right) = \prod_{i=1}^{n} \Pr\left(x_{(i)}\right), \qquad (33)$$

respectively. Finally, substituting (28)–(31) into (32) and (33), we can achieve Lemma 1.

APPENDIX B
PROOF OF THEOREM 1

Following the idea in [34], the BER expression of the in the proposed MST scheme can be derived as follows.

When $x_{(n)}$ is the "1" bit, the bit error would happen if the number of detected photons in the first slot is greater than or equal to those in the second slot of a BPPM symbol. Let ε_1 be the number of detected photons in the first slot of a BPPM symbol in the L_n, the conditional BER of the L_n given $x_{(n)} = 1$ can be written as (34) shown at the bottom of this page, where the conditional joint PMF of $\lambda_{n|1}$ and $\lambda_{n|2}$ given $x_{(n)} = 1$ is given in (35) shown at the bottom of this page. Besides, "Term 1" is the condition that the number of the detected photons in the first slot is less than that in the second slot. "Term 2" is the condition that the numbers of the detected photons in the first and the second slots are equal. Therefore, the random choice between "0" or "1" bits based on their prior probabilities will be made.

Similarly, when $x_{(n)}$ is the "0" bit, the bit error would happen if the number of detected photons in the second slot is greater than or equal to those in the first slot of a BPPM symbol. The conditional BER of the L_n given $x_{(n)} = 0$ can be written as (36) shown at the bottom of this page, where ε_2 is the number of detected photons in the second slot of a BPPM symbol in the L_n. In addition, the conditional joint PMF of $\lambda_{n|1}$ and $\lambda_{n|2}$ given $x_{(n)} = 0$ can be expressed as (37) shown at the top of the next page.

$$P_e \left(n \,\middle|\, x_{(n)} = 1\right)$$

$$= \sum_{x_{(1)}=0}^{1} \cdots \sum_{x_{(n-1)}=0}^{1} f_{\lambda_{n|1},\lambda_{n|2}} \left(\lambda_{n|1} = \mathcal{T}_{n|1}\left(x_{(1)},\ldots,x_{(n)}\right) + \lambda_n^b, \lambda_{n|2} = \mathcal{T}_{n|2}\left(x_{(1)},\ldots,x_{(n)}\right) + \lambda_n^b \,\middle|\, x_{(n)} = 1\right)$$

$$\times \sum_{\varepsilon_1=0}^{+\infty} \left[\underbrace{f_P\left(\varepsilon_1;\lambda_{n|1}\right) F_P\left(\varepsilon_1 - 1;\lambda_{n|2}\right)}_{\text{Term1}} + \underbrace{\Pr\left(x_{(n)} = 0\right) f_P\left(\varepsilon_1;\lambda_{n|1}\right) f_P\left(\varepsilon_1;\lambda_{n|2}\right)}_{\text{Term2}} \right] \qquad (34)$$

$$f_{\lambda_{n|1},\lambda_{n|2}} \left(\lambda_{n|1} = \mathcal{T}_{n|1}\left(x_{(1)},\ldots,x_{(n)}\right) + \lambda_n^b, \lambda_{n|2} = \mathcal{T}_{n|2}\left(x_{(1)},\ldots,x_{(n)}\right) + \lambda_n^b \,\middle|\, x_{(n)} = 1\right)$$

$$= \frac{f_{\lambda_{n|1},\lambda_{n|2}} \left(\lambda_{n|1} = \mathcal{T}_{n|1}\left(x_{(1)},\ldots,x_{(n)}\right) + \lambda_n^b, \lambda_{n|2} = \mathcal{T}_{n|2}\left(x_{(1)},\ldots,x_{(n)}\right) + \lambda_n^b\right)}{\Pr\left(x_{(n)} = 1\right)}$$

$$= \frac{1}{2^{n-1}} \qquad (35)$$

$$P_e \left(n \,\middle|\, x_{(n)} = 0\right)$$

$$= \sum_{x_{(1)}=0}^{1} \cdots \sum_{x_{(n-1)}=0}^{1} f_{\lambda_{n|1},\lambda_{n|2}} \left(\lambda_{n|1} = \mathcal{T}_{n|1}\left(x_{(1)},\ldots,x_{(n)}\right) + \lambda_n^b, \lambda_{n|2} = \mathcal{T}_{n|2}\left(x_{(1)},\ldots,x_{(n)}\right) + \lambda_n^b \,\middle|\, x_{(n)} = 0\right)$$

$$\times \sum_{\varepsilon_2=0}^{+\infty} \left[F_P\left(\varepsilon_2 - 1;\lambda_{n|1}\right) f_P\left(\varepsilon_2;\lambda_{n|2}\right) + \Pr\left(x_{(n)} = 1\right) f_P\left(\varepsilon_2;\lambda_{n|1}\right) f_P\left(\varepsilon_2;\lambda_{n|2}\right) \right] \qquad (36)$$

$$f_{\lambda_{n|1},\lambda_{n|2}}\left(\lambda_{n|1} = \mathcal{T}_{n|1}\left(x_{(1)},\dots,x_{(n)}\right) + \lambda_n^b, \lambda_{n|2} = \mathcal{T}_{n|2}\left(x_{(1)},\dots,x_{(n)}\right) + \lambda_n^b \,\middle|\, x_{(n)} = 0\right)$$

$$= \frac{f_{\lambda_{n|1},\lambda_{n|2}}\left(\lambda_{n|1} = \mathcal{T}_{n|1}\left(x_{(1)},\dots,x_{(n)}\right) + \lambda_n^b, \lambda_{n|2} = \mathcal{T}_{n|2}\left(x_{(1)},\dots,x_{(n)}\right) + \lambda_n^b\right)}{\Pr\left(x_{(n)} = 0\right)}$$

$$= \frac{1}{2^{n-1}} \qquad (37)$$

Finally, the BER expression of the L_n in the proposed MST scheme can be obtained as

$$P_e(n) = P_e\left(n \,\middle|\, x_{(n)} = 0\right) \Pr\left(x_{(n)} = 0\right)$$
$$+ P_e\left(n \,\middle|\, x_{(n)} = 1\right) \Pr\left(x_{(n)} = 1\right). \qquad (38)$$

Substituting (34) and (36) into (38), we can achieve Theorem 1.

REFERENCES

[1] W. Hu, Z. Wei, S. Popov, M. S. Leeson, M. Zhang, and T. Xu, "Non-coherent detection for ultraviolet communications with inter-symbol interference," *J. Lightw. Technol.*, vol. 38, no. 17, pp. 4699–4707, Sep. 2020.

[2] T. Cao, X. Gao, T. Wu, C. Pan, and J. Song, "Reflection-assisted non-line-of-sight ultraviolet communications," *J. Lightw. Technol.*, vol. 40, pp. 1953–1961, Apr. 2021.

[3] A. Vavoulas, H. G. Sandalidis, N. D. Chatzidiamantis, Z. Xu, and G. K. Karagiannidis, "A survey on ultraviolet C-band (UV-C) communications," *IEEE Commun. Surveys Tuts.*, vol. 21, no. 3, pp. 2111–2133, Jul.–Sep. 2019.

[4] R. Yuan and J. Ma, "Review of ultraviolet non-line-of-sight communication," *China Commun.*, vol. 13, no. 6, pp. 63–75, 2016.

[5] G. Wang, C. Gong, and Z. Xu, "Signal characterization for multiple access non-line of sight scattering communication," *IEEE Trans. Commun.*, vol. 66, no. 9, pp. 4138–4154, Sep. 2018.

[6] S. Arya and Y. H. Chung, "Spectrum sensing for optical wireless scattering communications over Málaga fading - a cooperative approach with hard decision fusion," *IEEE Trans. Commun.*, vol. 69, no. 7, pp. 4615–4631, Jul. 2021.

[7] C. Gong, K. Wang, Z. Xu, and X. Wang, "On full-duplex relaying for optical wireless scattering communication with on-off keying modulation," *IEEE Trans. Wireless Commun.*, vol. 17, no. 4, pp. 2525–2538, Apr. 2018.

[8] D. Han, Y. Gu, and M. Zhang, "Experimental study of an optimized PSP-OSTBC scheme with m-PPM in ultraviolet scattering channel for optical MIMO system," *Appl. Opt.*, vol. 56, no. 23, pp. 6564–6571, 2017.

[9] C. Gong and Z. Xu, "Temporal spectrum sensing for optical wireless scattering communications," *J. Lightw. Technol.*, vol. 33, no. 18, pp. 3890–3900, Sep. 2015.

[10] P. Luo, M. Zhang, D. Han, and Q. Li, "Performance analysis of short-range NLOS UV communication system using Monte Carlo simulation based on measured channel parameters," *Opt. Exp.*, vol. 20, no. 21, pp. 23489–23501, 2012.

[11] Q. He, Z. Xu, and B. M. Sadler, "Performance of short-range non-line-of-sight LED-based ultraviolet communication receivers," *Opt. Exp.*, vol. 18, no. 12, pp. 12226–12238, 2010.

[12] T. Nguyen and L. Lampe, "Coded multipulse pulse-position modulation for free-space optical communications," *IEEE Trans. Commun.*, vol. 58, no. 4, pp. 1036–1041, Apr. 2010.

[13] R. M. Gagliardi and S. Karp, *Optical Communications*, 2nd ed. Hoboken, NJ, USA: Wiley, 1995.

[14] H. Sugiyama and K. Nosu, "MPPM: A method for improving the band-utilization efficiency in optical PPM," *J. Lightw. Technol.*, vol. 7, no. 3, pp. 465–472, Mar. 1989.

[15] J. Song, T. Cao, and H. Zhang, "Performance analysis of a low-complexity nonorthogonal multiple access scheme in visible light communication downlinks using pulse modulations," *Intell. Converged Netw.*, vol. 2, no. 1, pp. 50–65, 2021.

[16] T. T. Nguyen and L. Lampe, "MPPM constellation selection for free-space optical communications," *IEEE Trans. Commun.*, vol. 60, no. 3, pp. 632–636, Mar. 2012.

[17] C. Gong, Q. Gao, and Z. Xu, "Signal detection for superposition transmission protocols for optical wireless scattering broadcast channel," *IEEE Trans. Wireless Commun.*, vol. 17, no. 8, pp. 5480–5493, Aug. 2018.

[18] G. Wang, C. Gong, Z. Jiang, and Z. Xu, "Multi-layer superimposed transmission for optical wireless scattering communication," *IEEE Photon. J.*, vol. 11, no. 5, pp. 1–14, May 2019.

[19] C. Gong and Z. Xu, "Non-line of sight optical wireless relaying with the photon counting receiver: A count-and-forward protocol," *IEEE Trans. Wireless Commun.*, vol. 14, no. 1, pp. 376–388, Jan. 2015.

[20] T. Cao, J. Song, and C. Pan, "Simplified closed-form single-scatter path loss model of non-line-of-sight ultraviolet communications in noncoplanar geometry," *IEEE J. Quantum Electron.*, vol. 57, no. 2, pp. 1–9, Feb. 2021.

[21] T. Wu, J. Ma, R. Yuan, P. Su, and J. Cheng, "Single-scatter model for short-range ultraviolet communication in a narrow beam case," *IEEE Photon. Technol. Lett.*, vol. 31, no. 3, pp. 265–268, Mar. 2019.

[22] R. J. Drost, T. J. Moore, and B. M. Sadler, "UV communications channel modeling incorporating multiple scattering interactions," *J. Opt. Soc. Amer. A*, vol. 28, no. 4, pp. 686–695, 2011.

[23] H. Ding, G. Chen, A. Majumdar, B. Sadler, and Z. Xu, "Modeling of non-line-of-sight ultraviolet scattering channels for communication," *IEEE J. Sel. Areas Commun.*, vol. 27, no. 9, pp. 1535–1544, Sep. 2009.

[24] Z. Xu, H. Ding, B. M. Sadler, and G. Chen, "Analytical performance study of solar blind non-line-of-sight ultraviolet short-range communication links," *Opt. Lett.*, vol. 33, no. 16, pp. 1860–1862, 2008.

[25] Y. Zuo, H. Xiao, J. Wu, Y. Li, and J. Lin, "A single-scatter path loss model for non-line-of-sight ultraviolet channels," *Opt. Exp.*, vol. 20, no. 9, pp. 10359–10369, 2012.

[26] T. Cao, X. Gao, T. Wu, C. Pan, and J. Song, "Single-scatter path loss model of LED-based non-line-of-sight ultraviolet communications," *Opt. Lett.*, vol. 46, no. 16, pp. 4013–4016, 2021.

[27] A. Bucholtz, "Rayleigh-scattering calculations for the terrestrial atmosphere," *Appl. Opt.*, vol. 34, no. 15, pp. 2765–2773, 1995.

[28] A. S. Zachor, "Aureole radiance field about a source in a scattering-absorbing medium," *Appl. Opt.*, vol. 17, no. 12, pp. 1911–1922, 1978.

[29] T. Cao, S. Chen, T. Wu, C. Pan, and J. Song, "Single-scatter channel impulse response model of non-line-of-sight ultraviolet communications," 2022, *arXiv:2209.00992*.

[30] Z. Ghassemlooy, W. Popoola, and S. Rajbhandari, *Optical Wireless Communications: System and Channel Modelling With MATLAB*. Boca Raton, FL, USA: CRC press, 2012.

[31] M. Audeh and J. Kahn, "Performance evaluation of L-pulse-position modulation on non-directed indoor infrared channels," in *Proc. Int. Conf. Commun.*, 1994, pp. 660–664.

[32] D. Tse and P. Viswanath, *Fundamentals of Wireless Communication*. New York, NY, USA: Cambridge Univ. Press, 2005.

[33] T. M. Cover and J. A. Thomas, *Elements of Information Theory*, 2nd ed. New York, NY, USA: Wiley, 2006.

[34] J. Hamkins and B. Moision, "Multipulse pulse-position modulation on discrete memoryless channels," *Interplanetary Netw. Prog. Rep.*, vol. 42, no. 161, pp. 1–13, 2005.